JOURNAL OF GEOPHYSICAL RESEARCH, VOL. 94, NO. B4, PAGES 4071–4087, APRIL 10, 1989

Large-Scale Ice Flow Over a Viscous Basal Sediment: Theory and Application to Ice Stream B, Antarctica

DOUGLAS R. MACAYEAL

Department of the Geophysical Sciences, The University of Chicago, Illinois

Recent seismic studies of ice stream B, Antarctica and field analysis of mid-latitude glacial deposits suggest that deformable basal sediments (e.g., water-saturated till) are important in determining ice sheet flow. If the ratio of till viscosity to effective ice viscosity is small, vertical shear associated with horizontal flow is confined to the deforming bed alone. Ice flow over a deformable bed is thus akin to that of floating ice shelves, because ice shelves flow over inviscid seawater. For some Antarctic ice streams, and possibly for portions of the late Wisconsin ice sheets in North America and Eurasia, basal drag associated with deforming basal sediment does not induce significant vertical gradients of horizontal velocity. Instead, basal drag affects the flow as if it were a horizontal body force balanced by longitudinal and transverse deviatoric stress gradients. Comparison of the observed flow of ice stream B to finite element simulations incorporating a viscous basal till suggest that a simple till rheology is sufficient to explain the current velocity profile. These simulations also highlight the importance of horizontal deviatoric stress in regions where driving stress and basal stress do not locally balance. While bed deformation is critical to ice stream existence, sensitivity tests suggest that ice shelf back pressure is still a crucial control affecting ice stream response to atmospheric and oceanic climate.

INTRODUCTION

Seismic soundings of ice stream B, Antarctica suggest that unconsolidated, water-saturated sediment at the ice stream bed may provide a lubricating layer on which the ice stream slides [*Blankenship et al.*, 1987; *Alley et al.*, 1986]. The viscosity of this layer implied by the force balance of the ice stream is much smaller than the effective viscosity of the ice [*Alley et al.*, 1987*b*]. This difference suggests that vertical shear needed to support the large horizontal surface velocity of the ice stream (exceeding 800 m a^{-1} in some locations) is confined entirely to the basal sediment [Alley et al., 1987*a*]. Although direct observations of the bed of ice stream B do not exist, such deformation is confirmed in other glacier settings. Observations conducted below Breiðamerkurjökul, Iceland, for example, indicate that 88% of the total vertical shear required to produce the surface flow is confined within the substratum [*Boulton and Jones*, 1979].

The presence of mobile subglacial sediment may answer the question of why ice streams exist [*Bentley*, 1987]. Concern over deformable sediment, however, is not confined to Antarctic and Greenland ice streams alone. Some reconstructions of the late Wisconsin Laurentide ice sheet, for example, display extensively flat lobes and ice plains on the southern margin [*Boulton et al.*, 1985]. Without bed deformation, ice flux sufficient to balance ablation would not have been plausible. Flat surface topography seen today in Antarctica where ice streams flow into floating ice shelves thus may characterize more general circumstances in which ice masses interact with basal sediment.

Paper number 88JB03848.
0148-0227/89/88JB-03848$05.00

In view of the subglacial conditions measured at ice stream B, and of possible conditions below past ice sheets, I investigate here the stress balance and flow of a large-scale ice stream resting on a viscous substrate. The governing equations are simplified to address a specific dynamic regime in which (1) the viscosity of subglacial sediment is assumed to be much smaller than the effective viscosity of ice and (2) the ice stream is assumed to be a thin shell resting on the Earth's surface (i.e., the ice thickness is much smaller than the horizontal span of the ice stream). Under these conditions, the stress balance is fundamentally similar to that of floating ice shelves in which the subglacial material is inviscid seawater. Distinctions between such ice streams and ice shelves are shown to be relatively minor; basal drag affects the ice stream, and ice shelves float in local hydrostatic equilibrium.

The approximate stress balance equations formulated for ice flowing over a viscous substrate or inviscid sea water is tested by comparing finite element simulations of ice stream B with observations of strain rate and velocity. Other demonstrations concerning, for example, the southern margin of the Laurentide ice sheet, were not conducted here owing to the lack of direct observations needed for model verification. Sensitivity tests involving modified ice stream parameters and basal sediment rheology are conducted to (1) determine the adequacy of a simple viscous rheology for the basal sediment, (2) determine if horizontal deviatoric stresses are important, (3) compare the relative roles of basal drag, ice shelf back pressure, and marginal shear stress in ice stream force balance, and (4) prioritize physical parameters for future study. In addition to these tests, the initial response of ice stream discharge to sudden climate changes affecting the Ross Ice Shelf is examined in a preliminary manner. The time-dependent behavior of the ice stream, however, is not considered in the present study. To do

so would require treating the mass balance of ice and the subglacial material [*Alley et al.*, 1987*b*]. This treatment can be included in future studies as a logical extension of the present inquiry.

The formulation of ice stream/ice shelf dynamics presented here stems from similar works by *Muszynski and Birchfield* [1987] and *MacAyeal and Barcilon* [1988] which describe consequences of small parameters on stress equilibrium (see also *Hutter* [1983]). In these previous studies, consequences of small geometric aspect ratio (thickness to horizontal span), or of the small difference between sea water density an ice density, are the principle concern. Here, I consider the additional consequences of small subglacial sediment strength. The characterization of deformable subglacial sediment (hereafter called till, for brevity) is based on the work of *Boulton and Jones* [1979] and *Alley et al.* [1987*b*]. For application of the finite element model to ice stream B, specified till thickness is based on detailed seismic reflection observations [*Blankenship et al.*, 1987]. Observations of surface velocity are used as the principal means of model verification [*Whillans et al.*, 1988; *Bindschadler et al.*, 1987]. Numerical methods and experiments described here are based on previous developments of ice shelf models [*MacAyeal and Lange*, 1988]. The coupled ice stream/ice shelf model developed here extends previous one-dimensional flow band models of ice streams [e.g., *Lingle and Brown*, 1987; *Van der Veen*, 1985; *Lingle*, 1984] to a two-dimensional, plan view geometry.

GOVERNING EQUATIONS

The behavior of an ice stream/ice shelf system is determined by the force, mass, and heat balances, and by imposed atmospheric, oceanic, and subglacial boundary conditions. The development of ice thickness over time, for example, is governed by mass accumulation and ice flow. Ice flow, in turn, is governed by the instantaneous ice thickness distribution, temperature-dependent rheology, and stress applied at the basal and lateral boundaries. Here I am concerned with the determination of ice flow alone, and in particular, the effects arising from deformable basal sediment or seawater. My goal is to describe the dominant stress balance and ice flow that result from arbitrary distributions of ice thickness, temperature, and basal sediment. The temporal evolution of this stress balance and flow, as dictated by mass flow and heat flow continuity, is a separate aspect of the system not considered in this study.

To simplify the stress equilibrium equations and attendant boundary constraints, I exploit two physical relationships suggested by observations of Antarctic ice streams. First, I assume that the horizontal length scale of flow variation is much larger than the vertical length scale, in other words, that the ice is a thin shell covering the Earth surface. Second, I assume that the viscosity of deforming basal till is much smaller than the effective viscosity of ice. This assumption is supported by observations of surface velocity, surface slope, and force balance on ice stream B [*Alley et al.*, 1987*b*]. The applicability of the second assumption to other active ice streams in Antarctica, however, awaits confirmation. Flow phenomena associated with circumstances in which these assumptions do not apply are not considered in the present study.

Suitable simplification of the stress equilibrium conditions following the above assumptions is performed in Appendix A and yields the following result:

$$\partial/\partial x(4H\nu_{av}e_{xx} + 2H\nu_{av}e_{yy}) + \partial/\partial y(2H\nu_{av}e_{xy}) = \begin{cases} -\tau_x + \rho g H(\partial z_s/\partial x) & \text{ice stream} \\ \rho g H(\partial z_s/\partial x) & \text{ice shelf} \end{cases} \quad (1)$$

$$\partial/\partial y(4H\nu_{av}e_{yy} + 2H\nu_{av}e_{xx}) + \partial/\partial x(2H\nu_{av}e_{yx}) = \begin{cases} -\tau_y + \rho g H(\partial z_s/\partial y) & \text{ice stream} \\ \rho g H(\partial z_s/\partial y) & \text{ice shelf} \end{cases} \quad (2)$$

All variables are defined in the notation list following Appendix B. The geometry and physical setting of the ice stream/ice shelf system to which (1) and (2) will be applied as a test are shown in Figures 1 and 2.

Equations (1) and (2) describe the vertically integrated balance of horizontal forces in the two horizontal dimensions x and y. The left-hand sides represent the effects of deviatoric stress components acting in the horizontal plane (typically these components are called the longitudinal, transverse, and horizontal shear stresses). The right-hand sides represent the effects of pressure gradients induced by free-surface slope and, for ice stream portions of the system, basal traction induced by till deformation. Basal traction appears not as a boundary condition, but rather as a horizontal body force integrated over the ice column. Equations (1) and (2) are written to display the

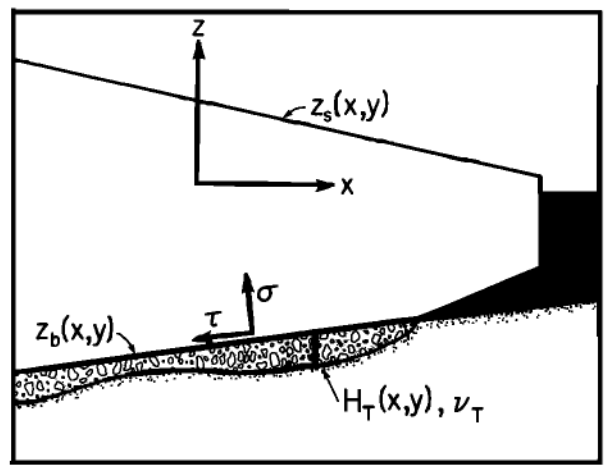

Fig. 1. Schematic cross section of an active ice stream in West Antarctica (the vertical dimension is exaggerated, and seawater is shown in black). Deformable subglacial till (of thickness H_T and viscosity ν_T) is present below the grounded ice stream. Here τ and σ represent tangential and normal stresses acting on the ice/till interface.

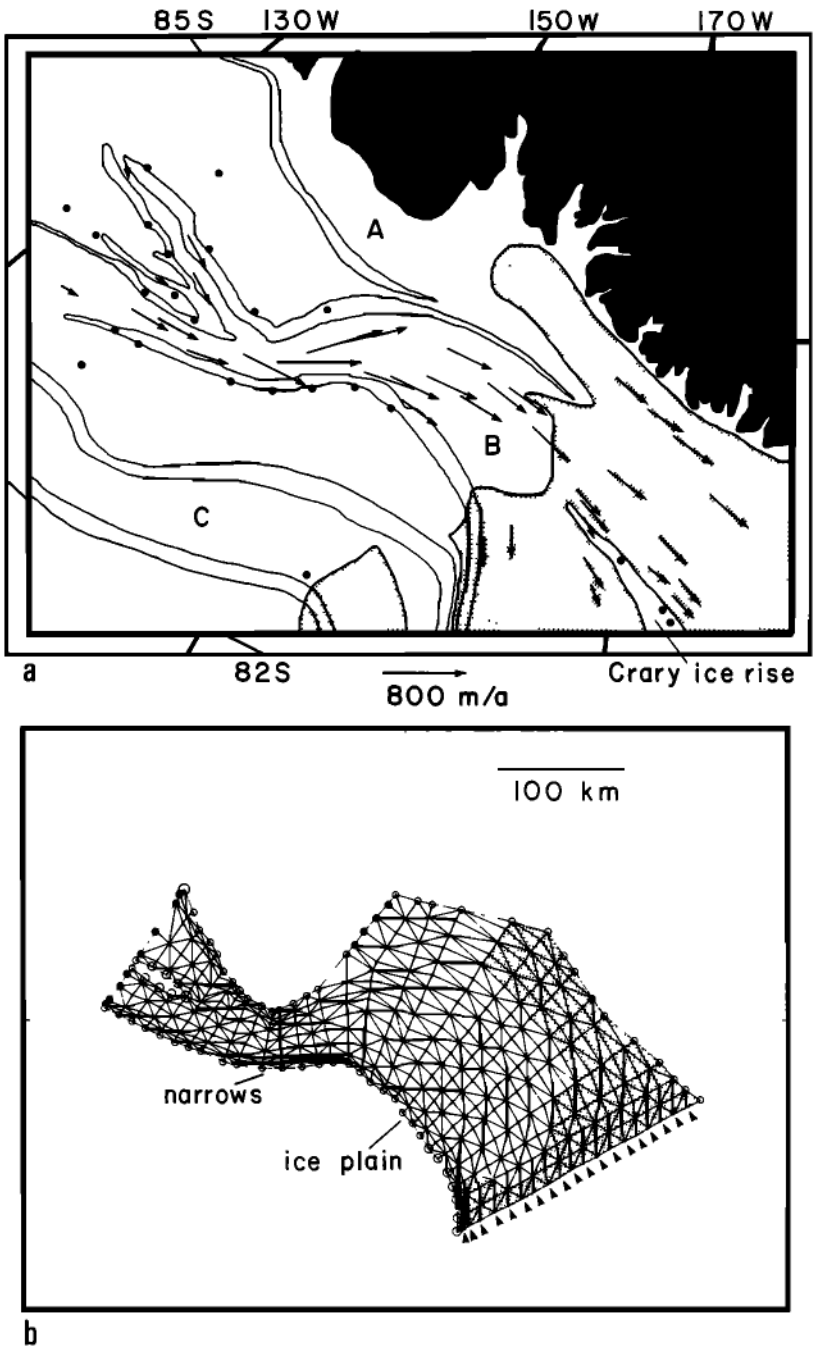

Fig. 2. (*a*) Map of ice stream B, Antarctica (adapted from *Shabtaie and Bentley* [1987]). Floating ice shelf is denoted by shading, the Transantarctic Mountains and the East Antarctic Ice Sheet are denoted by black. Observed velocity vectors (or solid circles where the velocity is negligible at the scale plotted) display strong velocity gradients between the ice stream and neighboring stagnant ice ridges [*Whillans et al.*, 1988; *Bindschadler et al.*, 1988]. Bands of severe surface crevassing and radar clutter along the margins of ice streams A, B, and C are outlined [*Vornberger and Whillans*, 1986; *Shabtaie and Bentley*, 1987]. (*b*) Finite element mesh used to simulate ice stream B. Shaded region is ice shelf, unshaded region is grounded. No-flow boundary conditions are applied at nodes indicated by open circles. Velocities are specified according to observations (Table 1) at nodes indicated by solid circles. Ice shelf back pressure is specified according to observations (Table 1) at nodes indicated by arrow heads.

similarities between the ice stream and the ice shelf portions of the system. Two distinctions between ice streams and ice shelves expressed in (1) and (2) are (1) that basal drag τ is zero for ice-shelf portions and (2) that the free-surface elevation z_s of the ice shelf is constrained by ice flotation ($z_s = (1 - \rho/\rho_w)H$).

A key property of the ice stream/ice shelf system not stated directly by (1) and (2) is the z independence of the horizontal velocity. This property is substantiated in Appendix A.

A precise definition of the flow regime for which (1) and (2) are valid involves two nondimensional numbers defined in Appendix A. This regime must satisfy

$$\epsilon << 1 \quad (3)$$

$$\delta^2 << 1 \quad (4)$$

where ϵ and δ^2 are defined by

$$\epsilon = (\nu_{To} H_o)/(\nu_o H_{To}) \quad (5)$$

$$\delta^2 = (H_o/L)^2 \quad (6)$$

and where scale values for ice viscosity ν_o, till viscosity ν_{To}, ice thickness H_o, till layer thickness H_{To}, and horizontal span L are defined in Appendix A (see Table A1). Here δ is the geometric aspect ratio of the ice stream/ice shelf system and is a measure of the vertical shear stress (deviatoric stress components T_{xz}' and T_{yz}') induced at the surface or base as a result of thickness gradients (subglacial bed topography is assumed also to posses a small geometric aspect ratio), ϵ is a measure of vertical shear stress induced by deformation of the basal till.

As discussed in Appendix A, (3) and (4) represent precise statements of the two key assumptions that lead to (1) and (2): (1) the viscosity of deforming basal sediment is assumed to be much smaller than that of the ice, and (2) ice thickness is assumed to be much smaller than the horizontal length scale of variations in the horizontal velocity components. The analysis presented by *Alley et al.* [1987*a*] suggests that $\epsilon \simeq 10^{-3}$ for ice stream B. Ice thickness and velocity observations on ice stream B and the Ross Ice Shelf suggest that $\delta^2 \simeq 10^{-2}$ [*Shabtaie and Bentley*, 1988; *Whillans et al.*, 1988]. Conditions (3) and (4) may be satisfied for several other ice streams, but direct observations are not available to confirm this.

Ice rheology associated with (1) and (2) is described by the incompressibility condition and a flow law that relates deviatoric stress to strain rate:

$$e_{xx} + e_{yy} + e_{zz} = 0 \quad (7)$$

$$\mathbf{T}' = 2\nu\mathbf{e} \quad (8)$$

$$\nu(e_{II}) = B(z)/(2e_{II}^{1-1/n}) \quad (9)$$

where e_{II} is the second invariant of the strain rate tensor, n is the power law flow exponent (in this study, $n=3$ is assumed), and $B(z)$ is a depth-dependent ice stiffness parameter which accounts for vertical variations in temperature, chemistry, and crystal fabric. These constitutive relations are based on laboratory creep tests and ice shelf field data analysis [*Thomas and MacAyeal*, 1982; *MacAyeal and Thomas*, 1986].

As a working hypothesis, tangential shear stress υ on the sloping ice/till interface is assumed to be a function of the ice velocity $\mathbf{u}$ and till layer thickness H_T:

$$\tau = -\nu_T/H_T \mathbf{u} \quad (10)$$

where $\mathbf{u}$ is evaluated at $z=z_b$, and ν_T and H_T are the viscosity and thickness of the deforming till layer, respectively. Equation (10) embodies two assumptions about till rheology and flow. First, till viscosity is assumed constant with depth (horizontal variations are allowed, however). Second, the horizontal velocity of the mobile till is assumed to be a linear function of z. In this circumstance, strain rates e_{xz} and e_{yz} within the till layer are $\frac{1}{2}u/H_T$ and $\frac{1}{2}v/H_T$, respectively. More complex parameterizations of deforming till rheology, which may include the effects of pore water pressure and grain size, are not considered here.

Conditions applied at lateral boundaries of the ice stream/ice shelf system can be either kinematic or dynamic. Appropriate kinematic conditions require specification of the vertically averaged horizontal velocity. Appropriate dynamic conditions require specification of the vertically integrated horizontal force. In this study, kinematic conditions are applied at the inland ice/ice stream boundaries and at lateral margins adjoining stagnant ice or coastline. Dynamic conditions are applied at an internal boundary contour that divides the Ross Ice Shelf where stress balance has been observed.

Depth-integrated conditions specified at the boundaries of the ice stream/ice shelf system are all that is necessary to solve (1) and (2). Actual velocity and force conditions at the boundaries, however, may posses strong vertical structure that is incompatible with the dynamics described by (1) and (2) and outlined in Appendix A. The effects of such inconsistency have been examined by *MacAyeal and Barcilon* [1988] in a simple physical example. They showed that incompatible vertical structure is winnowed from the flow within a short distance of the boundary by the stress balance constraints appropriate for the circumstance in which δ^2 is not small. Details of this winnowing process associated with ice stream B or other large-scale ice stream/ice shelf systems are not considered further in this paper.

Finite element solutions of (1) and (2) applicable to the current configuration of ice stream B are described in the following sections. Finite element methods used to produce them are summarized in Appendix B.

APPLICATION TO ICE STREAM B

To verify the applicability of (1) and (2) to large-scale Antarctic ice stream flow, numerical simulations were conducted to reproduce the present flow of ice stream B and a neighboring portion of the Ross Ice Shelf (Figure 2). Measured distributions of H and z_s, and boundary conditions determined from observations, were specified as model input. Model output consisted of velocity and strain rate distributions that satisfied (1) and (2) subject to the ice and till rheologies expressed by (7)-(10). This output was compared with the observed flow to evaluate model performance.

For simplicity, the vertical average of $B(z)$ was assumed to be uniform in the x,y domain (unless indicated otherwise) and ρ was assumed to be constant. The first assumption is appropriate under conditions in which the temperature-depth profile of the ice is horizontally uniform. Observed surface and basal temperatures support this simplification. The vertical average of $B(z)$ was fixed at the value given by the observed tem-

perature profile at J9 on the Ross Ice Shelf (1.6×10^8 Pa $s^{1/3}$) [*Clough and Hansen*, 1979]. The second assumption (of constant ρ) disregards the effects of lower ice density in the upper 80 m of the ice. Imprecision induced by this disregard is less than that induced by uncertainty (10-100 m) in the specified ice thickness.

Numerical Domain

My goal is to use extensive field measurements from ice stream B and the Ross Ice Shelf to constrain model input and to evaluate model performance. To meet this requirement, the model domain was limited to the area in which field measurements are concentrated. The finite element mesh, shown in Figure 2, encloses a 5×10^4 km^2 portion of ice stream B and the Ross Ice Shelf, and conforms with the flow regime determined from radio echo surveys [*Shabtaie and Bentley*, 1987; *Shabtaie et al.*, 1987].

The upstream boundary of the numerical domain crosses two tributaries of ice stream B which merge downstream of a stagnant island. This boundary is coincident with a transverse section along which ice thickness, surface elevation, and horizontal velocity are observed [*Whillans and Bindschadler*, 1988; *Shabtaie et al.*, 1988]. Deformable basal till possibly exists upstream of this boundary [*Alley et al.*, 1987c]. Extension of the finite element mesh into the inland ice, however, was not possible without abandoning the use of observed velocity as an upstream boundary condition. For the limited portion of ice stream A modeled, the upstream boundary coincides with a section near the grounding line where the ice thickness, surface elevation, and flow are measured.

The downstream boundary of the ice stream/ice shelf domain conforms with a section of the Ross Ice Shelf where total ice shelf back pressure is observed [*MacAyeal et al.*, 1987; *MacAyeal et al.*, 1989]. Application of this back pressure as a boundary condition duplicates the effects of the ice shelf not contained within the numerical domain and eliminates the need to extend the finite element mesh downstream to the ice front.

Lateral boundaries coincided with severely crevassed shear margins at the edges of the ice stream [*Bindschadler et al.*, 1987; *Shabtaie and Bentley*, 1987], or with the Transantarctic Mountains. Increased spatial resolution of the elements was applied near the lateral margins to better resolve strong horizontal shear and to examine sensitivity to strain heating, ice crystal fabric development, and the effects of ice fracture (which can be represented by reduced $B(z)$).

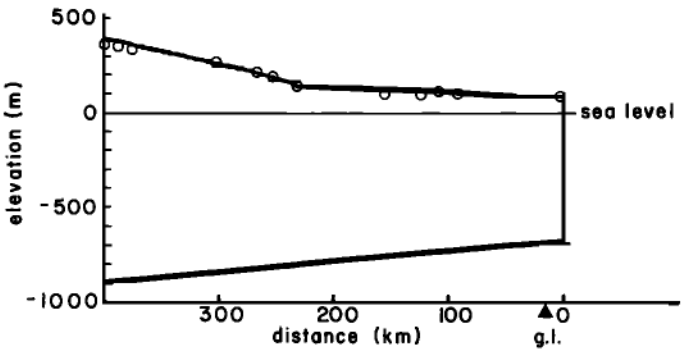

Fig. 3. Surface and base profiles along the longitudinal cross section (1 - 1', in Figure 4). Open circles denote observed surface elevations [Whillans et al., 1988; Bindschadler et al., 1988]. The grounding line is indicated by the point g.l.

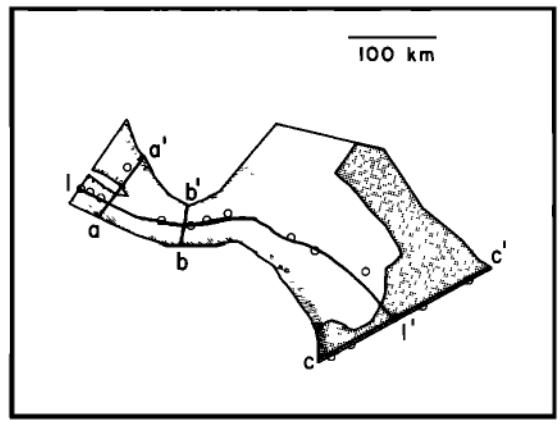

Fig. 4. Outline map of the numerical domain. Various cross sections along which simulated and observed velocities are compared are indicated by heavy lines. Open circles denote locations near the sections where velocities are observed. Shaded region denotes floating ice shelf. Patterned region denotes narrow bands of intense surface crevassing. These narrow bands are resolved with two rows of elements (see Figure 2), the outer of which is specified as having reduced ice stiffness in tests 3 and 7 (Table 2).

Ice thickness and surface elevation were specified from radar sounding data [*Shabtaie et al.*, 1987; *Shabtaie and Bentley*, 1988]. Small-scale thickness and basal surface variations were smoothed to avoid features that may reflect complexities of the basal regime not treated by (10). Figure 3 displays the surface and basal elevations along a longitudinal section (1 - 1', shown in Figure 4). The smoothed ice thickness is uniform along transverse sections.

Kinematic and dynamic boundary conditions applied at the margins are summarized in Table 1 and Figure 2. Observed velocity was specified at the upstream and lateral margins. Stress was specified along the downstream boundary using a scheme which reproduced the observed resistance of the Ross Ice Shelf:

$$\int \mathbf{T} \cdot \mathbf{n}\, dz = -\tfrac{1}{2}\rho_w g z_b^2 \mathbf{n} + \mathbf{F}(\lambda) \qquad (11)$$

where the lower and upper limits of integration are z_b and z_s, respectively, $\mathbf{n}$ is the outward pointing normal vector, λ is a coordinate defining position along the boundary, and $\mathbf{F}(\lambda)$ is the extra back pressure force (per unit length; defined as the difference between the total force and the force due to seawater pressure only) derived from observations (*MacAyeal et al.* [1987]; see also the correction by *MacAyeal et al.* [1989]). Total back pressure was partitioned into two parts to eliminate problems associated with imprecise ice thickness specification

TABLE 1. Model Boundary Conditions

Type of Boundary	Velocity		Force	
	Magnitude	Direction	Magnitude	Direction
Upstream end, inland ice/ice stream				
tributary B1[a]	425 ma^{-1}	perpendicular to boundary		
tributary B2[a]	370 ma^{-1}	perpendicular to boundary		
Ice stream/ice stream				
ice stream A[b]	250 ma^{-1}	perpendicular to boundary		
Downstream end, ice shelf/ice shelf[c]				
2			1.5×10^{12} N	125°
3 - 5			1.28	114.7
6 - 8			1.87	123.8
9			2.90	127.0
10			4.21	124.2
11			4.02	122.2
12 and 13			1.84	123.0
14 and 18			2.25	120.0
19 and 20			1.69	115.9

Force, observed F (*MacAyeal et al.* [1987]; see also corrections in the work by *MacAyeal et al.* [1989]).

[a] Observed velocity [*Whillans et al.*, 1988]. Tributary B1 is the southern most portion of the two ice stream branches that coalesce near the upstream end of ice stream B.

[b] Observed velocity [*Shabtaie et al.*, 1988].

[c] Nodes 1-21 extend from the lower left to upper right along downstream boundary in Figure 2. Force represents the integrated value of |F| applied at each node.

along the boundary (e.g., that which would arise if the measured total back pressure were applied to a boundary where the ice thickness of the model was less than that measured).

Adjustable Parameters

Several unconstrained parameters were adjusted empirically to facilitate better agreement between simulated and observed flow. In this regard, the numerical model was used as an inverse tool for parameter estimation. In the present study, ν_T/H_T was regarded as the major adjustable parameter. Independent studies of ice stream B suggest that ν_T/H_T should be in the range of 10^9 Pa s m^{-1} [*Alley et al.*, 1987*b*]. Parameters concerning the flow law of ice (equation (9)) may also be adjusted to improve fit. For simplicity, however, these were held fixed at values known to apply downstream on the Ross Ice Shelf.

COMPARISON BETWEEN MODEL AND OBSERVATION

Eight numerical simulations (described in Table 2) were conducted to verify model performance and determine sensitivity to unconstrained or poorly known parameters. Of all tests conducted, test 1 produced the best agreement between simulated and observed velocities. This agreement can be attributed to the specification of ν_T/H_T as a variable function of distance along the longitudinal axis (ν_T/H_T was assumed uniform in the transverse direction). In tests which specified ν_T/H_T as longitudinally constant, agreement could be achieved only in limited areas. The profile of ν_T/H_T chosen in test 1 is shown in Figure 5, and was determined by trial and error.

Simulated velocities of test 1 are shown in plan view in Figure 6 and in various sections in Figure 7. A direct comparison with observed velocities [*Whillans et al.*, 1988; *Bindschadler et al.*, 1987; *Bindschadler et al.*, 1988] is shown in Figure 8 (compare also Figures 2 and 6). The longitudinal velocity profile (Figure 7*a*) displays two local maxima. One velocity maximum occurs at the ice stream narrows (ice stream locations are labeled in Figure 2). The other velocity maximum occurs on

TABLE 2. Numerical Simulation Experiments

Test	Rationale	ν_T/H_T	|F|	B_{av} in Margins
1	best fit to observed velocities	Variable (Figure 5)	(Table 2)	1.6×10^8 Pa $s^{1/3}$
2	effect of constant ν_T/H_T	0.25×10^9 Pa s m^{-1}	as in test 1	as in test 1
3	ice softening in shear zones	as in test 1	as in test 1	1.6×10^7 Pa $s^{1/3}$ in boundary elements, unchanged elsewhere
4	no ice shelf back pressure	as in test 1	0.0 N	as in test 1
5	removal of the back pressure attributed to Crary Ice Rise	as in test 1	uniform (see text)	as in test 1
6	sensitivity to ice shelf back pressure	as in test 1	90% of values in test 1	as in test 1
7	sensitivity to shear margins	as in test 1	as in test 1	1.44×10^8 Pa $s^{1/3}$ in boundary elements
8	sensitivity to basal till rheology	90% of values in test 1	as in test 1	as in test 1

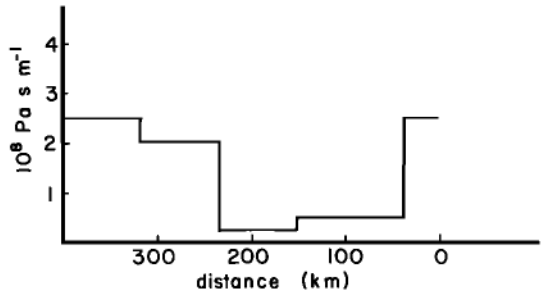

Fig. 5. The ν_T/H_T as a function of position on section 1 - 1' (Figure 4). This longitudinal variation produces a reasonable fit between simulated and observed velocity (test 1).

the ice plain (the region of low surface slope near the grounding line). Velocity decrease between the two maxima is associated with surface slope reduction and side boundary divergence at the exit of the ice stream narrows (Figures 2 and 3). The restraining influence of the Crary Ice Rise (as represented by the boundary conditions applied on the downstream boundary) causes velocities to decrease downstream of the second maximum.

Simulated and observed strain rates are displayed in Figure 9. The divergence of the horizontal velocity ($e_{xx} + e_{yy}$) is positive over most of the ice stream except in two regions (Figure 9*d*): (1) immediately downstream of the narrows and (2) within lateral shear margins upstream of the narrows. Downstream of the narrows, ($e_{xx} + e_{yy}$) is less than zero despite the divergence of the lateral ice stream boundaries. This is due to deceleration of longitudinal velocity (Figure 7*a*). The predominant strain rate pattern in the downstream part of the ice plain displays transverse stretching and longitudinal compression. This pattern results from strong back pressure concentration in the middle of the downstream boundary associated with the effects of Crary Ice Rise.

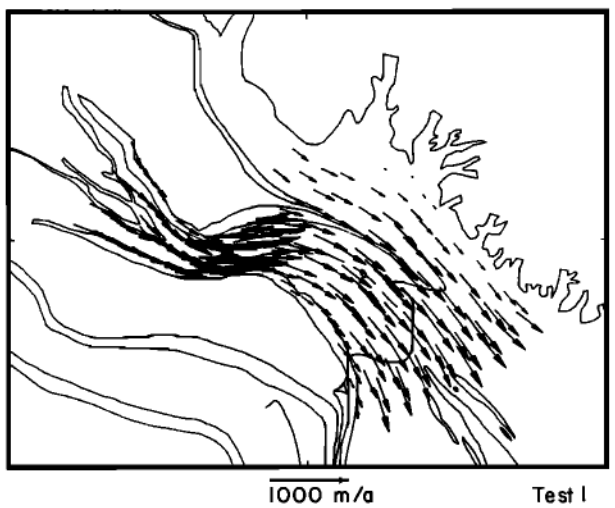

Fig. 6. Simulated ice velocity (test 1) plotted at every second node. The vectors are superimposed on the map of the region shown in Figure 2.

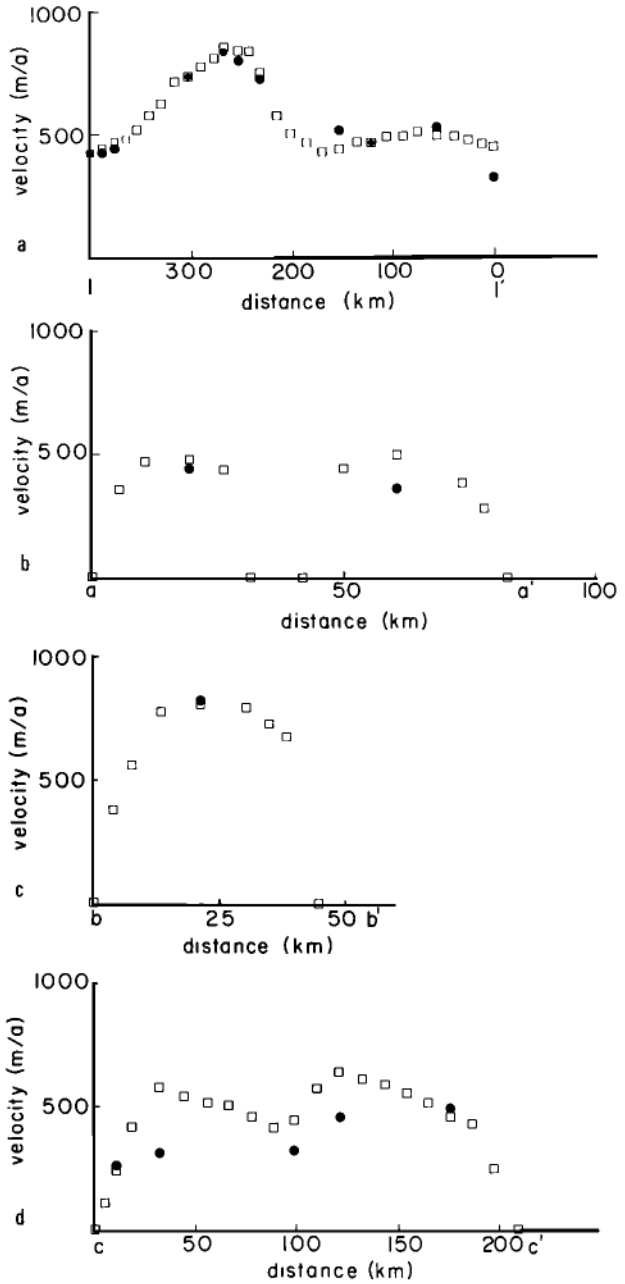

Fig. 7. Simulated velocity magnitude (open boxes) and observed velocity magnitude (solid circles) along (*a*) the longitudinal section (1 - 1', Figure 4) and (*b*)-(*d*) several transverse sections (a - a', b - b', and c - c', Figure 4).

Force and Mechanical Energy Balance

The question of whether horizontal gradients of the deviatoric stresses (the left-hand sides of equations (1) and (2)) are important in the ice stream force balance has yet to be answered conclusively [*Whillans*, 1987; *Bentley*, 1987; *Van der Veen*, 1987; *Whillans and Van der Veen*, 1988]. If they are not, as has been assumed in some previous studies of ice stream dynamics [e.g., *Alley et al.*, 1987*b*; *Lingle and Brown*, 1987], then driving stress and basal drag locally balance:

$$\rho g H \nabla z_s = \tau \qquad (12)$$

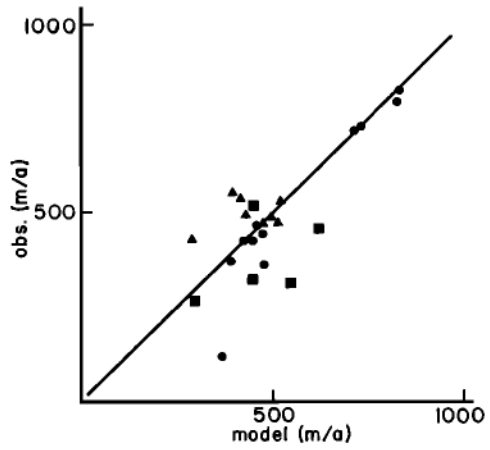

Fig. 8. Model and observed (obs.) velocity magnitude compared at 24 locations. Solid circles denote locations upstream of the narrows, solid triangles denote locations in the ice plain, and solid squares denote locations on the ice shelf.

In test 1 (Figure 10), driving stress and basal drag along the section 1 - 1' do not balance. Basal drag falls below driving stress by a factor of two or more in regions upstream of the narrows and in the downstream half of the ice plain. Surplus driving stress in these regions is balanced by resistance due to the funnelling effect at the narrows [*Whillans*, 1987] or to drag around the Crary Ice Rise. In the upstream half of the ice plain, basal drag exceeds local driving stress.

It was not possible to determine the complete force balance on a point-by-point basis using model data because deviatoric stress gradients are not given by the finite element algorithm at the same points as basal drag. The force balance was analyzed indirectly, however, by inspecting the mechanical energy budget. This budget is described in Appendix B and is displayed for test 1 in Table 3. Work done against basal drag accounts for only about 7% of total dissipation and is comparable to work done against horizontal gradients of the deviatoric stress (work done against internal friction). The predominant energy sources are work done by inland ice at the upstream boundary and gravitational potential energy released by ice thinning. Approximately half of the energy dissipated by the system is work done against back pressure at the downstream boundary.

Variable ν_T/H_T

If one accepts the characterization of basal drag in terms of till viscosity and thickness (equation (10)), then there are a number of effects which can contribute to both spatial and temporal variability in the ratio ν_T/H_T. Divergence of the horizontal ice velocity ($e_{xx} + e_{yy} > 0$), for example, tends to thin the till layer. This is because divergence of the depth-averaged till layer velocity, which is equal to half that of the ice under the current assumptions, will be positive. If not balanced by local till production through local erosion, till layer thinning by divergent horizontal transport would locally increase basal drag for a given ice velocity. Ice flow history in relation to till production rates can thus contribute to spatial variations in ν_T/H_T. Other factors contributing to variation of basal properties not considered in this study include pore water pressure, basal melting rate, till composition, and ice overburden.

To best fit observed velocities, ν_T/H_T was varied in test 1 as shown in Figure 5. Independent justification of this variation is beyond the scope of the present study. Consideration of till mass balance implied by the simulated ice stream flow, however, suggests one possible means for achieving the required variation in ν_T/H_T. Highest values of ν_T/H_T were required in the upstream third of the ice stream. Not considering the marginal shear zones, this region exhibits positive values of ($e_{xx} + e_{yy}$) that would thin the till layer over time if not balanced by till production (Figure 9*e*). Lowest values of ν_T/H_T are required downstream of the narrows where horizontal convergence is evident (Figure 9*e*).

As a comparison to test 1, test 2 was conducted with a spatially constant value of ν_T/H_T. The velocity of this test compares well (Figure 11) with observed flow in the upstream region. Downstream of the narrows, however, the velocity of test 2 falls to half of that observed.

Softening of Ice at Shear Margins

Radio echo sounding surveys of ice stream B and its environs reveal long, narrow bands of severe surface clutter (Figure 2) which correspond with the ice stream margin [*Shabtaie and Bentley*, 1987]. The width of these bands is approximately 3-10 km, and the length can extend over 500 km. Visually, these bands are seen as zones of chaotic surface crevassing [*Vornberger and Whillans*, 1986]. The transition between these bands and neighboring stagnant ice outside the ice streams is quite sharp (≈100 m) and suggests the presence of a surface strike-slip fault [*MacAyeal et al.*, 1986]. Field measurements show that 90% of the ice stream velocity is achieved by shear within the narrow zones of surface clutter [*Bindschadler et al.*, 1987] and suggest that ice strength may be reduced by fracture and strain heating.

To investigate how ice rheology within severely crevassed margins may affect ice stream flow, test 3 was conducted in which the vertical average of $B(z)$ was reduced in the elements at the margins of the ice stream domain. These elements correspond to the outside half of the patterned region depicted in Figure 4. Results of this test (Figure 11) show a significant velocity increase in the narrows where resistive drag by the funnelling effect is strongest.

Ice Shelf Back Pressure

Perhaps the most appropriate application of the ice stream/ice shelf model developed here is to investigate ice shelf back pressure as a restraint on ice stream discharge. Unlike basal till properties or marginal softening discussed above, back pressure is controlled directly by oceanic and atmospheric processes, and may be expected to change over the next century in association with CO_2 warming. The downstream boundary condition applied in test 1 reproduces the observed back pressure derived from field measurements (Table 1). About half of

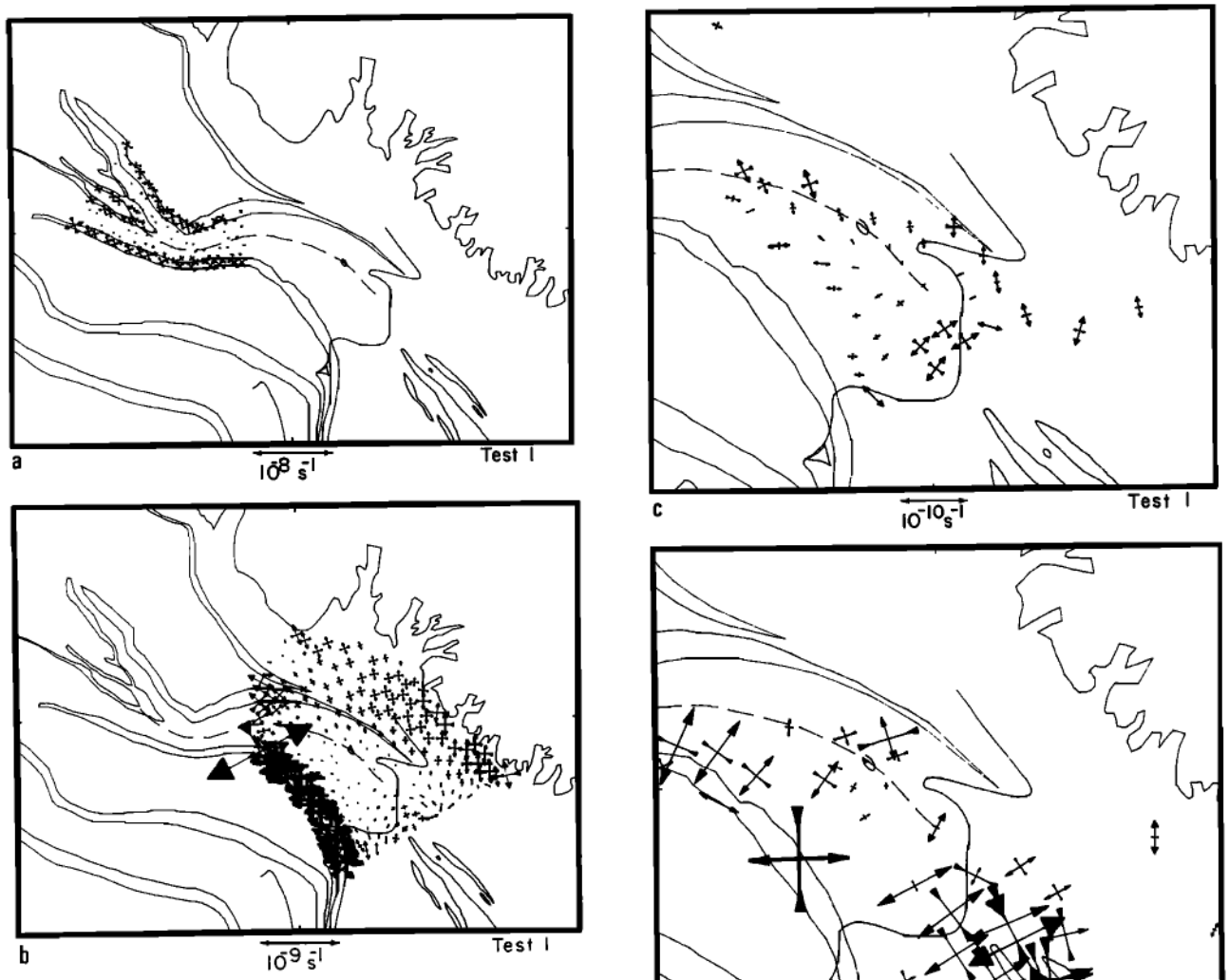

Fig. 9. Principal axes of the horizontal strain rate tensor in every second element produced by test 1 (outward pointing arrow heads denote extension, inward pointing arrow heads denote compression). To display the wide range of strain rate variation, a larger plotting scale was used in the region upstream of the narrows (Figure 9*a*) than in the region downstream of the narrows (Figure 9*b*). Close-up view of simulated strain rates on the ice plain (test 1). To emphasize the central ice plain where field observations are not impeded by severe crevassing and where strain rate magnitude is low, strain rates with magnitudes in excess of 5.0×10^{-11} s^{-1} are not plotted. Observed strain rates in the ice plain [*Bindschadler et al.*, 1987]. Elements in which net horizontal convergence of the simulated flow of test 1 are indicated by an asterisk. Convergence downstream of the narrows occurs despite divergence of the ice stream sides and may be responsible for basal till deposition.

the extra back pressure F defined in (11) is due to the Crary Ice Rise which lies downstream of the boundary and is concentrated in the middle section of the boundary. The result of this concentration has been discussed previously in reference to the strain rate and velocity patterns of test 1 (Figures 6, 7, and 9).

To determine the overall effect of ice shelf back pressure, two tests were conducted in which |F| was reduced. In test 4, F was set to zero. In test 5, the portion of F attributed to the Crary Ice Rise alone was eliminated (|F| was assumed uniform along the boundary and its integral along the boundary was set to 2.0×10^{13} N). In both tests, velocity in the ice plain, and the total volume discharge across the grounding line, were greatly increased (Figure 11). This result confirms the critical relation-

Fig. 9. (continued)

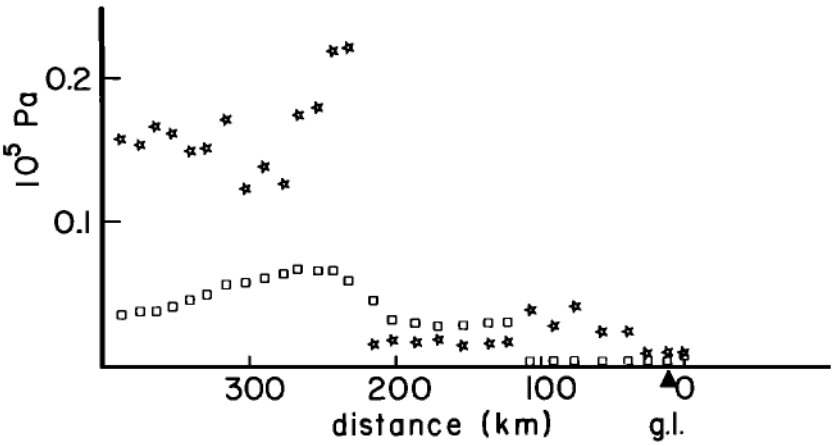

Fig. 10. Comparison between driving stress magnitude ($|\rho g H \nabla z_s|$, open stars) and basal stress magnitude ($|\tau|$, open boxes) in test 1.

ship between ice stream stability and ice rise restrictions described by *Thomas et al.* [1979].

Parameter Sensitivity

To assess relative sensitivity of ice stream discharge to various controls, tests 6-8 were conducted in which conditions used in test 1 were individually varied by a small increment. In test 6, the magnitude of back stress due to ice shelf back pressure $|F|$ was reduced by 10%. In test 7, the vertical average of B was reduced by 10% in elements along the shear margins. In test 8, ν_T/H_T was reduced from the values shown in Figure 5 by 10%. Ice stream discharge ($km^3\ a^{-1}$) produced by each test is given in Table 4.

Comparison of tests 6-8 shows that ice stream discharge is sensitive to all parameters varied and is most sensitive to ice shelf back pressure. Assuming that till conditions and shear margin rheology are not directly controlled by climate, ice shelf back pressure appears to be the most significant effect linking ice stream discharge with oceanic and atmospheric climate.

The relationship between ice shelf back pressure and ice stream discharge demonstrated in tests 4-6 is not seen in models of ice stream behavior that assume a balance between basal drag and driving stress. *Alley et al.* [1987*b*], for example, show that a reduction in back pressure (represented by sudden ice shelf thinning at the grounding line) produces a time-dependent thickness adjustment that propagates slowly upstream as a damped wave. Without account of longitudinal deviatoric stress in their model, ice velocity change is tied to ice thickness change, and ice thickness change requires time dependence. In the present study, the force balance includes longitudinal deviatoric stress, and this inclusion gives rise to the possibility of instantaneous ice velocity changes in response to grounding line conditions. Models that do not account for horizontal deviatoric stress may not represent short-term response to climatic change correctly.

TABLE 3. Mechanical Energy Budget for Test 1

Term	Value, W
Sinks	
Work done against basal drag	-9.06×10^8
Work done against deviatoric stresses	-2.57×10^9
Work done against sea water pressure on sloping ice shelf base	-8.76×10^8
Work done to push grounded ice up a basal slope	-2.25×10^9
Work done against ice shelf back pressure	-7.37×10^9
Sources	
Work done on the system by inland ice	9.66×10^9
Release of gravitational potential energy	4.28×10^9

CONCLUSION

If the viscosity of a deforming subglacial sediment is small compared with that of ice, horizontal flow of the ice above the sediment is dynamically similar to ice shelf flow. Vertical shear strain rates needed to support large horizontal ice velocities are confined within the subglacial sediment. In this circumstance, basal drag and horizontal deviatoric stress gradients can contribute equally in balancing gravitational driving stress. Kinship between ice stream and ice shelf dynamics thus provides a natural avenue toward their unification in numerical models of ice sheet response to climatic forcing. Although in the present study, subglacial till has been treated as a thin layer of incompressible viscous fluid, more complex till rheology incorporating, for example, pore water pressure, basal heat balance, and deformation history would evoke similar consequences. Improved parameterization of the deformable bed is important

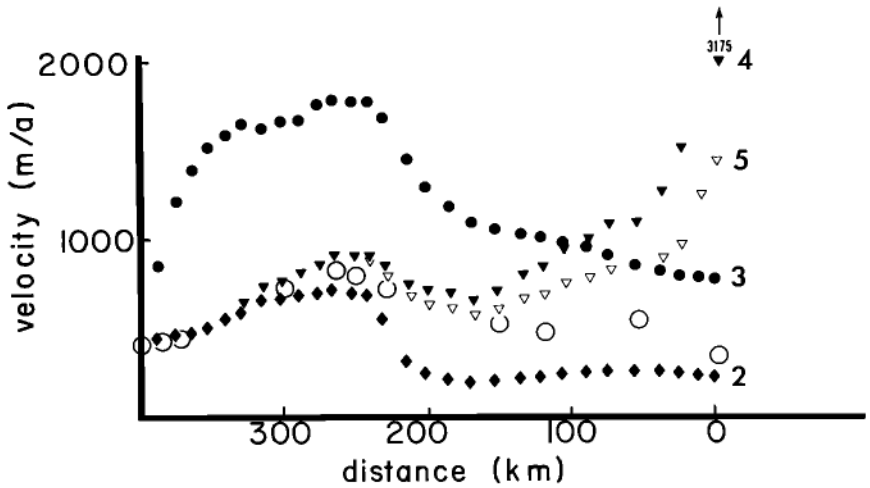

Fig. 11. Longitudinal velocity profiles along section I - I' (Figure 4) for tests 2-5. Open circles denote observed velocity.

primarily in determining long-term time evolution of the ice/sediment system.

Finite element simulations of ice stream B, Antarctica, and comparison of their results with extensive field observations confirm the formulation of ice stream/ice shelf dynamics developed here. The best agreement between simulation and observation was obtained by specifying the ratio of till viscosity to till layer thickness ν_T/H_T as a spatially variable function (high upstream of the narrows and low on the ice plain). This variation can be attributed to a number of mechanisms including till continuity constraints discussed by *Alley et al.* [1987*b*]. If the ice stream has been active for an extended period and if the till production rate (subglacial erosion) is relatively low, then the till-layer thickness in regions of horizontal ice divergence will have thinned. Divergence of the horizontal velocity ($e_{xx} + e_{yy} > 0$) is observed today upstream of the narrows (Figures 2 and 9*d*), where the highest values of ν_T/H_T were specified.

Sensitivity tests examining the relative roles of basal till strength, ice softening in severely crevassed shear bands, and ice shelf back pressure show comparable effects on ice stream discharge. Ice shelf back pressure is closely linked to atmospheric and oceanic climate, and thus may be more important than till conditions or shear bands in initiating ice stream response to short-term climate change. Feedback between ice stream flow and basal till conditions, such as that produced by till transport continuity [*Alley et al.*, 1987*b*] or by basal heat balance, is undoubtedly important in long-term ice stream evolution. In future research, this feedback can be incorporated into the model developed here.

TABLE 4. Sensitivity of Ice Stream Discharge to Various Parameters

Test	Discharge $km^3\ a^{-1}$	Difference With Test 1, $km^3\ a^{-1}$
1	72	
6 (reduced back pressure)	86	14
7 (shear margin softening)	76	4
8 (reduced ν_T/H_T)	75	3

The discharge value computed is higher in all cases than that observed (47 $km^3\ a^{-1}$; *MacAyeal et al.* [1989]) because simulated velocities and specified thickness are higher than observed at the downstream boundary.

APPENDIX A: DERIVATION OF GOVERNING EQUATIONS

The goal of this derivation is to simplify the stress equilibrium equations and associated boundary conditions to account for the physical regime in which ϵ and δ^2 defined in (5) and (6) are small. This regime complies with situations in which (1) the viscosity of the deforming subglacial material is smaller that of ice and (2) ice thickness is much smaller than the horizontal length scale of horizontal ice velocity variation (in addition, the Earth's surface is assumed to have a slope not exceeding δ). To achieve the goal, I perform the following four steps. First, the stress equilibrium equations and associated boundary conditions are expressed in terms of nondimensional variables having values assumed to be less than or equal to one. Second, the small size of ϵ and δ^2 are exploited using the calculus of perturbations in which each variable is expressed as a power series in ϵ [*Courant and Hilbert*, 1953]. Third, the zero-order approximation to the stress equilibrium equations and boundary conditions generated by the calculus of perturbations is shown to imply that the zero-order horizontal velocity is z independent (e.g., that nondimensional vertical shear strain rates are much less than one). Fourth, the first-order approximation is used to generate nondimensional forms of (1) and (2).

Nondimensional Stress Equilibrium Equations

The stress equilibrium and associated boundary conditions are expressed in terms of nondimensional variables by dividing

the dimensional variables by appropriate scale values described in Table A1. Each nondimensional variable in the equations is assumed to be of order one or less. The size of each term in the nondimensional equations is assumed to be less than or equal to the size of any nondimensional factors which appear. To avoid excessively complex notation, all variables in Appendix A (this section) are assumed nondimensional and have the same notation as their dimensional counterparts used in all other sections of this paper. The choice of scales applied in Table A1 constitutes an assumption about the physical regime being studied. Here, the scales are chosen to focus on the small ϵ, small δ^2 regime which is assumed to reflect the large-scale behavior of an ice stream/ice shelf system. Flow features for which these scales are not appropriate will be disregarded in this study.

The scale assigned to e_{xz} and e_{yz} require explanation. This relatively large scale ($\delta^{-1}U/L$) represents conditions in which vertical shear strain associated with horizontal ice flow is confined predominantly to the ice rather than the subglacial bed. This a priori scale assignment represents an apparent conflict with the desired result of the derivation: that e_{xz} and e_{yz} are indeed negligible compared to other strain rate components. This apparent conflict is resolved by the calculus of perturbations. The zero-order approximation to the stress equilibrium equations and associated boundary conditions derived below will show that the order one terms of e_{xz} and e_{yz} are identically zero. Nonzero terms of e_{xz} and e_{yz} appear in the first-order approximation, and this implies that the nondimensional size of e_{xz} and e_{yz} is equal to or less than ϵ.

The stress balance equations are written below in terms of nondimensional variables (geometry and physical setting are shown in Figures 1 and 2; scales of variables are defined in Table A1):

$$-\Gamma(\partial p/\partial x) + \partial/\partial x(\nu e_{xx}) + \partial/\partial y(\nu e_{xy}) + \delta^{-2}\partial/\partial z(\nu e_{xz}) = 0 \quad \text{(A1)}$$

$$\partial/\partial x(\nu e_{yx}) - \Gamma(\partial p/\partial y) + \partial/\partial y(\nu e_{yy}) + \delta^{-2}\partial/\partial z(\nu e_{yz}) = 0 \quad \text{(A2)}$$

$$\partial/\partial x(\nu e_{zx}) + \partial/\partial y(\nu e_{zy}) - \Gamma(\partial p/\partial z + 1) + \partial/\partial z(\nu e_{zz}) = 0 \quad \text{(A3)}$$

for $z_b < z < z_s$. Dynamic boundary conditions at the ice/atmosphere interface $z = z_s(x,y,t)$ are

$$-(\partial z_s/\partial x)(\nu e_{xx} - \Gamma p) - (\partial z_s/\partial y)(\nu e_{xy}) + \delta^{-2}\nu e_{xz} = 0 \quad \text{(A4)}$$

$$-(\partial z_s/\partial x)(\nu e_{yx}) - (\partial z_s/\partial y)(\nu e_{yy} - \Gamma p) + \delta^{-2}\nu e_{yz} = 0 \quad \text{(A5)}$$

$$-(\partial z_s/\partial x)(\nu e_{zx}) - (\partial z_s/\partial y)(\nu e_{zy}) + \nu e_{zz} - \Gamma p = 0 \quad \text{(A6)}$$

Dynamic boundary conditions at the ice/till or ice/sea water interface at $z = z_b(x,y,t)$ are

TABLE A1. Scales Used in Dimensional Analysis of the Stress Balance Equations

Variable	Scale	Value of Scale Assumed to Apply to Ice Stream B
B	B_o	1.6×10^8 Pa $s^{1/3}$
e_{xx}	U/L	1.6×10^{-9} s^{-1}
e_{yy}	U/L	1.6×10^{-9} s^{-1}
e_{zz}	U/L	1.6×10^{-9} s^{-1}
e_{xy}	U/L	1.6×10^{-9} s^{-1}
e_{xz}	$\delta^{-1}U/L$	1.6×10^{-8} s^{-1}
e_{yz}	$\delta^{-1}U/L$	1.6×10^{-8} s^{-1}
H	H_o	1000 m
H_T	H_{To}	10 m
p	$\rho g H_o$	9.0×10^6 Pa
u	U	1.6×10^{-5} m s^{-1}
v	U	1.6×10^{-5} m s^{-1}
w	δU	1.6×10^{-6} m s^{-1}
x	L	10^4 ν
y	L	10^4 m
z	H_o	10^3 m
z_s	H_o	10^3 m
z_b	H_o	10^3 m
δ	H_o/L	10^{-1}
ϵ	$(\nu_{To}H_o)/(\nu_o H_{To})$	1.7×10^{-3}
Γ	$\rho g H_o/[B_o(U/L)^{1/3}]$	48
ν	$\nu_o = B_o/[2(U/L)^{1-1/3}]$	5.8×10^{13} Pa s
ν_T	ν_{To}	10^9 Pa s
σ	$\rho g H_o$	9.0×10^6 Pa
τ_x	$\nu_{To}U/H_{To}$	1.6×10^3 Pa
τ_y	$\nu_{To}U/H_{To}$	1.6×10^3 Pa
τ_z	$H_{To}/L\ \nu_{To}U/H_{To}$	1.6 Pa

$$(\partial z_b/\partial x)(\nu e_{xx} - \Gamma p) + (\partial z_b/\partial y)(\nu e_{xy}) - \delta^{-2}\nu e_{xz}$$

$$= \begin{cases} \delta^{-2}\epsilon\tau_x - \Gamma\sigma(\partial z_b/\partial x) & \text{ice stream} \\ (\rho_w/\rho)\Gamma z_b(\partial z_b/\partial x) & \text{ice shelf} \end{cases} \quad \text{(A7)}$$

$$(\partial z_b/\partial x)(\nu e_{yx}) + (\partial z_b/\partial y)(\nu e_{yy} - \Gamma p) - \delta^{-2}\nu e_{yz}$$

$$= \begin{cases} \delta^{-2}\epsilon\tau_y - \Gamma\sigma(\partial z_b/\partial y) & \text{ice stream} \\ (\rho_w/\rho)\Gamma z_b(\partial z_b/\partial y) & \text{ice shelf} \end{cases} \quad \text{(A8)}$$

$$(\partial z_b/\partial x)(\nu e_{zx}) + (\partial z_b/\partial y)(\nu e_{zy}) - \nu e_{zz} + \Gamma p$$

$$= \begin{cases} \epsilon\tau_z + \Gamma\sigma & \text{ice stream} \\ -(\rho_w/\rho)\Gamma z_b & \text{ice shelf} \end{cases} \quad \text{(A9)}$$

For grounded ice, (A7)-(A9) express continuity of tangential and normal stress, τ and σ respectively, at the ice/till interface. For floating ice, these conditions express the continuity of normal stress $(\rho_w/\rho)\Gamma z_b$ at the ice/sea water interface.

As a working hypothesis, tangential shear stress τ on the sloping ice/till interface is assumed to be a function of ice velocity $\mathbf{u}$ and till layer thickness H_T:

$$\tau = -\nu_T/H_T\,\mathbf{u} \quad \text{(A10)}$$

where $\mathbf{u}$ is evaluated at $z=z_b$, and ν_T and H_T are the nondimensional viscosity and nondimensional thickness of the deforming till layer, respectively.

The constitutive relation for the ice represents incompressible, power law flow:

$$e_{xx} + e_{yy} + e_{zz} = 0 \quad \text{(A11)}$$

$$\mathbf{T} = \nu\mathbf{e} - \Gamma p \quad \text{(A12)}$$

where p is the nondimensional pressure and the nondimensional effective viscosity is defined by

$$\nu(e_{II}) = B(z)/(e_{II}^{1-1/n}) \quad \text{(A13)}$$

and where e_{II} is the second invariant of the nondimensional strain rate tensor, $n=3$ is the power law flow exponent, and $B(z)$ is the nondimensional ice stiffness parameter. The power law flow exponent is nondimensional and of order one in the dimensional form of (A13), thus no scale factors are necessary to convert n to its nondimensional form.

Nondimensional Parameters

Three nondimensional parameters appear in (A1)-(A13): Γ, δ, and ϵ. Assignment of scales to these three parameters constitutes the precise statement of the flow regime to which this derivation is addressed. Γ is the ratio of the horizontal stress induced by gravity to the stress required to deform the ice at the reference strain rate U/L. Γ appears in (A36) and (A37), which are derived below, as a coefficient of the surface elevation gradient. Γ is thus a measure of the importance of ice thickness gradients to ice flow. For scales representing the flow regime considered in this paper (Table A1), Γ is a large number. Here $\delta^2=(H_o/L)^2$ is the square of the aspect ratio and is assumed to be 10^{-2}. The presence of ϵ as a coefficient of τ in (A7)-(A9) suggests that ϵ measures the strength of ice/till coupling. The definition of ϵ given in (5) can be written

$$\epsilon = (\nu_{To}U/H_{To})/(\nu_o U/H_o) \quad \text{(A14)}$$

In this alternative definition, ϵ is interpreted as the ratio of the stress required to deform the subglacial till with vertical shear (U/H_{To}) to the stress required to deform the ice with vertical shear (U/H_o). In this paper, ϵ is assumed to be 10^{-3}.

Perturbation Series Expansion

Systematic approximations to the governing equations listed above in the small ϵ, small δ^2 limits are developed using the calculus of perturbations [*Courant and Hilbert*, 1953]. To simplify this procedure and avoid dealing with two small parameters, ϵ is equated with δ^2. This simplification is possible because scales chosen in the present study imply that ϵ is smaller than δ^2. Approximations are developed by expressing all variables as a power series of the small parameter ϵ:

$$e_{xz} = e_{xz}^{(0)} + \epsilon e_{xz}^{(1)} + \epsilon^2 e_{xz}^{(2)} + \ldots \quad \text{(A15)}$$

$$\vdots$$

Substituting these expressions into the governing equations written above, and requiring coefficients of each power of ϵ to cancel separately, yields the zero- and first-order approximations to the governing equations discussed below. The goal of the following analysis is to determine equations that govern the zero-order variables. The small size of e assumed in the present study suggests that terms beyond zero order can be disregarded. To determine how these zero-order terms behave, it is necessary, however, to examine the governing equations at both zero and first order.

Zero-Order Approximation

The zero-order equations are, for the interior,

$$\partial/\partial z(\nu^{(0)}e_{xz}^{(0)}) = 0 \quad z_b<z<z_s \quad \text{(A16)}$$

$$\partial/\partial z(\nu^{(0)}e_{yz}^{(0)}) = 0 \quad z_b<z<z_s \quad \text{(A17)}$$

$$\partial/\partial x(\nu^{(0)}e_{xx}^{(0)}) + \partial/\partial y(\nu^{(0)}e_{xy}^{(0)}) + \partial/\partial z(\nu^{(0)}e_{xz}^{(0)}) - \Gamma(\partial p^{(0)}/\partial z + 1) = 0 \quad z_b < z < z_s \tag{A18}$$

for the ice/air interface

$$e_{xz}^{(0)} = 0 \quad z = z_s \tag{A19}$$

$$e_{yz}^{(0)} = 0 \quad z = z_s \tag{A20}$$

$$-(\partial z_s/\partial x)(\nu^{(0)}e_{xx}^{(0)}) - (\partial z_s/\partial y)(\nu^{(0)}e_{xy}^{(0)}) + \nu^{(0)}e_{zz}^{(0)} - \Gamma p^{(0)} = 0 \quad z = z_s \tag{A21}$$

and for the ice/till or ice/sea water interface,

$$e_{xz}^{(0)} = 0 \quad z = z_b \tag{A22}$$

$$e_{yz}^{(0)} = 0 \quad z = z_b \tag{A23}$$

$$(\partial z_b/\partial x)(\nu^{(0)}e_{xx}^{(0)}) + (\partial z_b/\partial y)(\nu^{(0)}e_{xy}^{(0)}) - \nu^{(0)}e_{zz}^{(0)} + \Gamma p^{(0)} = \begin{cases} \Gamma\sigma^{(0)} & \text{ice stream } z = z_b \\ -(\rho_w/\rho)\Gamma z_b & \text{ice shelf } z = z_b \end{cases} \tag{A24}$$

The solution to the zero-order equations is found by integrating (A16)-(A18) over z and using the boundary conditions (equations (A22)-(A24)) to evaluate the result. This solution is

$$e_{xz}^{(0)} = 0 \quad z_b \le z \le z_s \tag{A25}$$

$$e_{yz}^{(0)} = 0 \quad z_b \le z \le z_s \tag{A26}$$

$$\Gamma p^{(0)} = \Gamma(z_s - z) + \nu^{(0)}e_{zz}^{(0)} \quad z_b \le z \le z_s \tag{A27}$$

$$\sigma^{(0)} = z_s - z_b \quad \text{ice stream} \tag{A28}$$

$$z_b = \rho(\rho - \rho_w)^{-1} z_s \quad \text{ice shelf} \tag{A29}$$

The zero-order solution (equations (A25)-(A29)) indicates that the nondimensional strain rate components e_{xz} and e_{yz} are less than or equal to ϵ. To be explicit,

$$e_{xz} = 0 + \epsilon e_{xz}^{(1)} + \epsilon^2 e_{xz}^{(2)} + \ldots \tag{A30}$$

$$e_{yz} = 0 + \epsilon e_{yz}^{(1)} + \epsilon^2 e_{yz}^{(2)} + \ldots \tag{A31}$$

Although e_{xz} and e_{yz} were assigned much larger scales than e_{xx}, e_{yy}, e_{zz}, and e_{xy} (Table A1), the zero-order analysis above establishes that the nondimensional size of e_{xz} and e_{yz} is much smaller than one. In addition to z independence, the zero-order solution specifies that (1) zero-order horizontal strain rates ($e_{xx}^{(0)}$, $e_{yy}^{(0)}$, $e_{zz}^{(0)}$, and $e_{xy}^{(0)}$) do not vary with z (this follows from negligible $e_{xz}^{(0)}$ and $e_{yz}^{(0)}$); (2) zero-order pressure $p^{(0)}$ increases linearly with z; (3) zero-order normal stress $\sigma^{(0)}$ across the ice/till interface is glaciostatic; and (4) ice shelf portions of the system float in hydrostatic equilibrium.

First-Order Approximation

The zero-order solution described above provides only a partial description of the zero-order flow. The horizontal variation of $e_{xx}^{(0)}$, $e_{yy}^{(0)}$, $e_{zz}^{(0)}$, and $e_{xy}^{(0)}$ are not described. To determine the zero-order horizontal stress balance, it is necessary to extend the analysis to first order. The first-order stress balance equations and boundary conditions needed to accomplish this goal are

$$-\Gamma(\partial p^{(0)}/\partial x) + \partial/\partial x(\nu^{(0)}e_{xx}^{(0)}) + \partial/\partial y(\nu^{(0)}e_{xy}^{(0)}) = -\partial/\partial z(\nu^{(0)}e_{xz}^{(1)}) \quad z_b < z < z_s \tag{A30}$$

$$\partial/\partial x(\nu^{(0)}e_{yx}^{(0)}) - \Gamma(\partial p^{(0)}/\partial y) + \partial/\partial y(\nu^{(0)}e_{yy}^{(0)}) = -\partial/\partial z(\nu^{(0)}e_{yz}^{(1)}) \quad z_b < z < z_s \tag{A31}$$

$$-(\partial z_s/\partial x)(\nu^{(0)}e_{xx}^{(0)} - \Gamma p^{(0)}) - (\partial z_s/\partial y)(\nu^{(0)}e_{xy}^{(0)}) = -\nu^{(0)}e_{xz}^{(1)} \quad z = z_s \tag{A32}$$

$$-(\partial z_s/\partial x)(\nu^{(0)}e_{yx}^{(0)}) - (\partial z_s/\partial y)(\nu^{(0)}e_{yy}^{(0)} - \Gamma p^{(0)}) = -\nu^{(0)}e_{yz}^{(1)} \quad z = z_s \tag{A33}$$

$$(\partial z_b/\partial x)(\nu^{(0)}e_{xx}^{(0)} - \Gamma p^{(0)}) + (\partial z_b/\partial y)(\nu^{(0)}e_{xy}^{(0)}) = \begin{cases} \nu^{(0)}e_{xz}^{(1)} + \tau_x^{(0)} - \Gamma\sigma^{(0)}(\partial z_b/\partial x) & \text{ice stream } z = z_b \\ \nu^{(0)}e_{xz}^{(1)} + (\rho_w/\rho)\Gamma z_b(\partial z_b/\partial x) & \text{ice shelf } z = z_b \end{cases} \tag{A34}$$

$$(\partial z_b/\partial y)(\nu^{(0)}e_{yy}^{(0)} - \Gamma p^{(0)}) + (\partial z_b/\partial x)(\nu^{(0)}e_{yx}^{(0)}) = \begin{cases} \nu^{(0)}e_{yz}^{(1)} + \tau_y^{(0)} - \Gamma\sigma^{(0)}(\partial z_b/\partial y) & \text{ice stream } z = z_b \\ \nu^{(0)}e_{yz}^{(1)} + (\rho_w/\rho)\Gamma z_b(\partial z_b/\partial y) & \text{ice shelf } z = z_b \end{cases} \tag{A35}$$

Integration of (A30) and (A31) over z, application of the Leibnitz rule for differentiation of integrals, and substitution for $\nu^{(0)}e_{xz}^{(1)}$ and $\nu^{(0)}e_{yz}^{(1)}$ (evaluated at z_s and z_b) using the boundary conditions (equations (A32)-(A35)) give expressions for the zero-order horizontal stress balance:

$$\partial/\partial x(2H\nu_{av}^{(0)}e_{xx}^{(0)} + H\nu_{av}^{(0)}e_{yy}^{(0)}) + \partial/\partial y(H\nu_{av}^{(0)}e_{xy}^{(0)}) = \begin{cases} -\tau_x^{(0)} + \Gamma H(\partial z_s/\partial x) & \text{ice stream} \\ \Gamma H(\partial z_s/\partial x) & \text{ice shelf} \end{cases} \tag{A36}$$

$$\partial/\partial y(2H\nu_{av}^{(0)}e_{yy}^{(0)} + H\nu_{av}^{(0)}e_{xx}^{(0)}) + \partial/\partial x(H\nu_{av}^{(0)}e_{yx}^{(0)}) = \begin{cases} -\tau_y^{(0)} + \Gamma H(\partial z_s/\partial y) & \text{ice stream} \\ \Gamma H(\partial z_s/\partial y) & \text{ice shelf} \end{cases} \quad \text{(A37)}$$

where $H = z_s - z_b$ is the nondimensional ice thickness and $\nu_{av}^{(0)}$ is the vertical average of $\nu^{(0)}$.

Equations (A36) and (A37) govern the behavior of the ice stream/ice shelf system at points (x,y) sufficiently distant from lateral margins. The result of the small ϵ approximation is to eliminate vertical stress balance as an independent unknown. The weak, order ϵ vertical shear stresses distribute the basal shear stress through the ice column. As a result, this effect becomes indistinguishable from a fictitious horizontal body force.

APPENDIX B: FINITE ELEMENT IMPLEMENTATION

The finite element method was used to solve the time-independent elliptic boundary value operator represented by (1) and (2). This method permits variable spatial resolution where desired (such as within the severely crevassed lateral margins) and has performed favorably in simulations of ice shelf flow [*MacAyeal and Lange*, 1988].

Equations (1) and (2) are expressed as integral equations which incorporate dynamic boundary conditions (specification of stress) by the method of weighted residuals [*Lapidus and Pinder*, 1982]. This conversion is displayed for the x momentum balance as follows. Strain rate components appearing in (1) are written in terms of velocity components u and v (see the notation section) to avoid having to satisfy a compatibility condition. This compatibility condition would insure that the three strain rate components appearing in (1) represent a continuous velocity distribution. Equation (1) is multiplied by an arbitrary weighting function $R(x,y)$, and the result is integrated over the entire area of the coupled ice stream/ice shelf system (all variables in Appendix B are dimensional):

$$\int_{(A_f+A_g)} \{ R\partial/\partial x(\nu_{av}H(4\partial u/\partial x + 2\partial v/\partial y)) + R\partial/\partial y(\nu_{av}H(\partial u/\partial y + \partial v/\partial x)) \}\, da = \int_{(A_f+A_g)} R[\rho g H(\partial z_s/\partial x)]\, da - \int_{A_g} R\tau_x\, da \quad \text{(B1)}$$

where A_g is the ice stream region (grounded), A_f is the ice shelf region (floating), and da is a differential element of area in the horizontal plane. If $\mathbf{u}=(u,v)$ is a solution to (B1) for arbitrary weighting functions $R(x,y)$, then it is also a solution of (1). Integrating (B1) by parts, expressing z_s in terms of H ($z_s = H + z_b$ for grounded ice, or $z_s = (1 - \rho/\rho_w)H$ for floating ice), and incorporating dynamic boundary conditions (specification of boundary stress) gives the following integral constraint that forms the basis of the numerical model described in this paper:

$$\int_{(A_f+A_g)} \{ (\partial R/\partial x)(\nu_{av}H(4\partial u/\partial x + 2\partial v/\partial y)) + (\partial R/\partial y)(\nu_{av}H(\partial u/\partial y + \partial v/\partial x)) \}\, da = \int_{(A_f+A_g)} [\tfrac{1}{2}\rho g H^2(\partial R/\partial x)]\, da + \int_{A_f} (\rho^2/\rho_w) g H R(\partial H/\partial x)\, da - \int_{A_f} \rho g H(\partial z_b/\partial x) R\, da + \int_{A_g} R\tau_x\, da - \int_S R\mathbf{T}\cdot\mathbf{n}_x\, ds \quad \text{(B2)}$$

S is the area of the boundary section where stresses $\mathbf{T}$ are applied as boundary conditions, ds is a differential element of area in the vertical plane, and $\mathbf{n}_x$ is the x component of the outward pointing unit vector along S. At boundaries where kinematic conditions are applied, the solution $\mathbf{u}$ is not free to vary in such a way as to minimize the weighted residual expressed by (B2). $R(x,y)$ along these portions of the boundary is thus set to zero without loss of generality.

Equation (B2) may be treated in a similar manner to yield

$$\int_{(A_f+A_g)} \{ (\partial Q/\partial y)(\nu_{av}H(4\partial v/\partial y + 2\partial u/\partial x)) + (\partial Q/\partial x)(\nu_{av}H(\partial u/\partial y + \partial v/\partial x)) \}\, da = \int_{(A_f+A_g)} [\tfrac{1}{2}\rho g H^2(\partial Q/\partial y)]\, da + \int_{A_f} (\rho^2/\rho_w) g H Q(\partial H/\partial y)\, da - \int_{A_f} \rho g H(\partial z_b/\partial y) Q\, da + \int_{A_g} Q\tau_y\, da - \int_S R\mathbf{T}\cdot\mathbf{n}_y\, ds \quad \text{(B3)}$$

Equations (B2) and (B3) can be clarified in terms of the mechanical energy balance if the weighting functions R and Q are replaced with velocities u and v in the x direction and y direction, respectively. The sum of terms on the left-hand side of the two equations represents viscous energy dissipation. The sum of corresponding terms on the right-hand sides represent, respectively, (1) work done against gravity by vertical mass redistribution in both floating and grounded areas, (2) work done against seawater pressure at the bottom of floating ice, (3) work done against gravity to push ice up a sloping basal surface (alternatively, the second and third terms on the right-hand side can be combined to represent work done against a pressure gradient force proportional to $\rho g H \nabla z_s$), (4) work done against stress at the ice/till interface, and, finally, (5) work

done against imposed forces at the boundaries (such as sea water pressure at an ice front).

Equations (B2) and (B3) are discretized by dividing the area of the ice stream/ice shelf system into triangular elements of arbitrary geometry (as shown in Figure 2). A restriction on this breakup is that the grounding line fall on element boundaries. Variables H, z_s, z_b, u, v, R, Q (the arbitrary weighting function in equation (B3)), τ_x, and τ_y are approximated as piecewise linear functions, and their variation is represented by values at vertices (nodes) of the triangular elements; ν_{av} is approximated by a piecewise constant function (constant within each element). With these representations, and with the requirement that nodal values of R and Q be arbitrary, (B2) and (B3) are converted to a system of nonlinear algebraic equations for the nodal values of u and v, and for the elemental values of ν_{av}. This system is solved using an iterative technique to ensure that ν_{av} satisfies the flow law (equations (8) and (9)) [*MacAyeal and Thomas*, 1986].

The numerical procedure described above was tested by comparing it to exact solutions and by monitoring the mechanical energy budget described above. An exact solution of (1) and (2) can be derived for a simple ice stream configuration in which the following conditions are satisfied: flow is laminar through a straight channel of uniform width, ice thickness and basal elevation are constant, free-slip conditions are applied at sides, seawater pressure is applied as a downstream boundary condition (on a terminal ice wall), and τ is constant (as opposed to a function of $\mathbf{u}$). The longitudinal spreading rate given by this exact solution is

$$e_L = e_{is}\gamma \tag{B4}$$

where

$$\gamma = [1 + 2(1 - \rho/\rho_w)^{-1}(\Delta/H) - (\rho_w/\rho)(1 - \rho/\rho_w)^{-1}(\Delta/H)^2 - 2\tau d(H^2\rho g(1 - \rho/\rho_w))^{-1}]^3 \tag{B5}$$

where Δ is the difference between H and the minimum thickness to remain grounded, d is the longitudinal distance between the points where γ is evaluated and the terminal ice wall, and e_{is} is the longitudinal spreading rate of an ice shelf of thickness H given by

$$e_{is} = ((4B_{av})^{-1}\rho g(1 - \rho/\rho_w)H)^3 \tag{B6}$$

where B_{av} is the vertical average of $B(z)$.

Without exact solutions available for more complex ice stream/ice shelf configurations such as ice stream B, model performance was checked by ensuring balance of the mechanical energy budget. Typical model runs achieve balance to within 0.3% of the net energy dissipation.

NOTATION

A_f region of floating ice in the x,y plane
A_g area of grounded ice in the x,y plane
$B(z)$ ice stiffness parameter, Pa $s^{-1/3}$.
B_{av} vertical average of $B(z)$, Pa $s^{-1/3}$.
$\mathbf{e}$ strain rate tensor, s^{-1}.
e_{II} second invariant of $\mathbf{e}$, s^{-1}.
e_{xx} $(\partial u/\partial x)$ xx component of $\mathbf{e}$, s^{-1}.
e_{yy} $(\partial v/\partial y)$ yy component of $\mathbf{e}$, s^{-1}.
e_{zz} $(\partial w/\partial z)$ zz component of $\mathbf{e}$, s^{-1}.
e_{xy} $\frac{1}{2}(\partial u/\partial y + \partial v/\partial x)$ xy component of $\mathbf{e}$, s^{-1}.
e_{xz} $\frac{1}{2}(\partial u/\partial z + \partial w/\partial x)$ xz component of $\mathbf{e}$, s^{-1}.
e_{yz} $\frac{1}{2}(\partial v/\partial z + \partial w/\partial y)$ yz component of $\mathbf{e}$, s^{-1}.
e_L longitudinal spreading rate of ideal ice stream, s^{-1}.
e_{is} longitudinal spreading rate of ideal ice shelf, s^{-1}.
$\mathbf{F}$ extra force at downstream boundary, N m^{-1}.
g gravitational acceleration, 9.81 m s^{-2}.
$H(x,y,t)$ ice thickness, m.
$H_T(x,y,t)$ till thickness, m.
n flow law exponent, 3, nondimensional.
p pressure, Pa.
$Q(x,y)$ arbitrary weighting function, m s^{-1}.
$R(x,y)$ arbitrary weighting function, m s^{-1}.
S contour defining boundary in the x,y plane.
$\mathbf{T}$ stress tensor, Pa.
$\mathbf{T}'$ deviatoric stress tensor, Pa.
t time, s.
$\mathbf{u}$ horizontal velocity, m s^{-1}.
u x component of ice velocity, m s^{-1}.
v y component of ice velocity, m s^{-1}.
w z component of ice velocity, m s^{-1}.
x horizontal coordinate, m.
y horizontal coordinate, m.
z vertical coordinate, m.
$z_s(x,y,t)$ surface elevation, m.
$z_b(x,y,t)$ basal elevation, m.
Δ excess ice thickness above buoyancy, m.
δ aspect ratio, nondimensional.
ϵ till/ice strength ratio, nondimensional.
γ spreading rate amplification factor, nondimensional.
Γ $[\rho g H_o/(B_o(U/L)^{1/n})]$ stress ratio number, nondimensional.
Γ^* contour defining downstream boundary (defined by *MacAyeal et al.*, [1987]).
$\nu(e_{II})$ effective ice viscosity, Pa s.
ν_{av} vertical average of $\nu(e_{II})$, Pa s.
ν_T till viscosity, Pa s.
ρ ice density, 917 kg m^{-3}.
ρ_w sea water density, 1027 kg m^{-3}.
σ normal force per unit area at ice/till boundary, Pa.
τ tangential force per unit area at ice/till boundary, Pa.
τ_x x component of basal stress, Pa.
τ_y y component of basal stress, Pa.
τ_z z component of basal stress, Pa.

Acknowledgments. This research was supported by the National Science Foundation DPP 85 09451. The derivation of the governing equations arises from correspondence with Kolumban Hutter, who

refereed in 1986 an unpublished manuscript on a similar subject, and from discussions with Victor Barcilon. Participants of the Siple Coast project in Antarctica (notably Richard B. Alley, Charles R. Bentley, Robert A. Bindschadler, Sion Shabtaie, and Ian M. Whillans, among others) provided discussion and data at early stages of model development. Dean R. Lindstrom provided assistance in computer code development and testing. Charles R. Bentley, Craig S. Lingle, George W. Platzman, and Richard Frolich were instrumental in clarifying the derivations presented in Appendix A and in improving the overall quality of the paper.

REFERENCES

Alley, R. B., D. D. Blankenship, C. R. Bentley, and S. T. Rooney, Deformation of till beneath ice stream B, West Antarctica, *Nature*, *322*(6074), 57-59, 1986.

Alley, R. B., D. D. Blankenship, C. R. Bentley, and S. T. Rooney, Till beneath ice stream B, 3, Till deformation: Evidence and implications, *J. Geophys. Res.*, *92*(B9), 8921-8929, 1987a.

Alley, R. B., D. D. Blankenship, S. T. Rooney, and C. R. Bentley, Till beneath ice stream B, 4, A coupled ice-till flow model, *J. Geophys. Res.*, *92*(B9), 8931-8940, 1987b.

Alley, R. B., D. D. Blankenship, S. T. Rooney, and C. R. Bentley, Continuous till deformation beneath ice sheets, in *The Physical Basis of Ice Sheet Modelling* , edited by E. D. Waddington and J. S. Walder, IAHS Publ. No. 170, pp. 81-91, IAHS Press, Wallingford, United Kingdom, 1987c.

Bentley, C. R., Antarctic ice streams: A review, *J. Geophys. Res.*, *92*(B9), 8843-8858, 1987.

Bindschadler, R. A., S. N. Stephenson, D. R. MacAyeal, and S. Shabtaie, Ice dynamics at the mouth of ice stream B, Antarctica, *J. Geophys. Res.*, *92*(B9), 8885-8894, 1987.

Bindschadler, R. A., D. R. Lindstrom, D. R. MacAyeal, E. Roberts, and S. N. Stephenson, Data report for the Siple Coast project, *Rep. NASA TM-100708*, National Aeronautics and Space Administration, Greenbelt, Maryland, 1988.

Blankenship, D. D., C. R. Bentley, S. T. Rooney, and R. B. Alley, Till beneath ice stream B, 1, Properties derived from seismic travel times, *J. Geophys. Res.*, *92*(B9), 8903-8911, 1987.

Boulton, G. S., and A. S. Jones, Stability of temperate ice caps and ice sheets resting on beds of deformable sediment, *J. Glaciol.*, *24*(90), 29-43, 1979.

Boulton, G. S., G. D. Smith, A. S. Jones, and J. Newsome, Glacial geology and glaciology of the last mid-latitude ice sheets, *J. Geol. Soc. London*, *142*, 447-474, 1985.

Clough, J. W., and B. L. Hansen, The Ross Ice Shelf project, *Science*, *203*(4379), 422-434, 1979.

Courant, R., and D. Hilbert, *Methods of Mathematical Physics*, 560 pp., Wiley-Interscience, New York, 1953.

Hutter, K., *Theoretical Glaciology*, 510 pp., D. Reidel, Hingham, Mass., 1983.

Lapidus, L., and G. F. Pinder, *Numerical Solution of Partial Differential Equations in Science and Engineering*, 677 pp., John Wiley, New York, 1982.

Lingle, C. S., A numerical model of interactions between a polar ice stream and the ocean: Application to ice stream E, West Antarctica, *J. Geophys. Res.*, *89*(C3), 3523-3549, 1984.

Lingle, C. S., and T. J. Brown, A subglacial aquifer bed model and water pressure dependent basal sliding relationship for a West Antarctic ice stream, in *Dynamics of the West Antarctic Ice Sheet*, edited by C. J. Van der Veen and J. Oerlemans, pp. 249-285, D. Reidel, Hingham, Mass., 1987.

MacAyeal, D. R., and R. H. Thomas, The effects of basal melting on the present flow of the Ross Ice Shelf, Antarctica, *J. Glaciol.*, *32*(110), 72-86, 1986.

MacAyeal, D. R., S. Shabtaie, C. R. Bentley, and S. D. King, Formulation of ice shelf dynamic boundary conditions in terms of a Coulomb rheology, *J. Geophys. Res.*, *91*(B8), 8177-8191, 1986.

MacAyeal, D. R., R. A. Bindschadler, S. Shabtaie, S. Stephenson, and C. R. Bentley, Force, mass, and energy budgets of the Crary Ice Rise complex, Antarctica, *J. Glaciol.*, *33*(114), 218-230, 1987.

MacAyeal, D. R., R. A. Bindschadler, S. Shabtaie, S. Stephenson, and C. R. Bentley, Correction to Force, mass, and energy budgets of the Crary Ice Rise Complex, Antarctica, *J. Glaciol.*, in press, 1989.

MacAyeal, D. R., and V. Barcilon, Ice-shelf response to ice-stream discharge fluctuations, I, Unconfined ice tongues, *J. Glaciol.*, *34*(116), 121-127, 1988.

MacAyeal, D. R., and M. A. Lange, Ice-shelf response to ice-stream discharge fluctuations, II, Ideal rectangular ice shelf, *J. Glaciol.*, *34*(116), 128-135, 1988.

Muszynski, I., and G. E. Birchfield, A coupled marine ice-stream-ice-shelf model, *J. Glaciol.*, *33*(113), 3-15, 1987.

Shabtaie, S., and C. R. Bentley, West Antarctic ice streams draining into the Ross Ice Shelf: Configuration and mass balance, *J. Geophys. Res.*, *92*(B2), 1311-1336, 1987.

Shabtaie, S., and C. R. Bentley, Ice thickness map of the West Antarctic ice stream by radar sounding, *Ann. Glaciol.*, *11*, in press, 1988.

Shabtaie, S., I. M. Whillans, and C. R. Bentley, The morphology of ice streams A, B, and C, West Antarctica, and their environs, *J. Geophys. Res.*, *92*(B9), 8865-8883, 1987.

Shabtaie, S., C. R. Bentley, R. A. Bindschadler, and D. R. MacAyeal, Mass balance studies of ice streams A, B, and C, and possible surging behavior of ice stream B, *Ann. Glaciol.*, *11*, in press, 1988.

Thomas, R. H., and D. R. MacAyeal, Derived characteristics of the Ross Ice Shelf, Antarctica, *J. Glaciol.*, *28*(100), 397-412, 1982.

Thomas, R. H., T. J. O. Sanderson, and K. E. Rose, Effect of climatic warming on the West Antarctic ice sheet, *Nature*, *277*, 355-358, 1979.

Van der Veen, C. J., Response of a marine ice sheet to changes at the grounding line. *Quat. Res.*, *24*, 257-267, 1985.

Van der Veen, C. J., Longitudinal stresses and basal sliding: a comparative study, in *Dynamics of the West Antarctic Ice Sheet*, edited by C. J. Van der Veen and J. Oerlemans, pp. 223-248, D. Reidel, Hingham, Mass., 1987.

Vornberger, P. L., and I. M. Whillans, Surface features of ice stream B, Marie Byrd Land, West Antarctica, *Ann. Glaciol.*, *8*, 168-170, 1986.

Whillans, I. M., Force budget of ice sheets, in *Dynamics of the West Antarctic Ice Sheet*, edited by C. J. Van der Veen and J. Oerlemans, pp. 17-36, D. Reidel, Hingham, Mass., 1987.

Whillans, I. M., and R. H. Bindschadler, Mass balance of ice stream B, *Ann. Glaciol.*, *11*, in press, 1988.

Whillans, I. M., and C. J. van der Veen, Force Budget, I, General theory, *J. Glaciol.*, in press, 1988.

Whillans, I. M., J. Bolzan, and S. Shabtaie, Velocity of ice streams B and C, Antarctica, *Ann. Glaciol.*, *11*, in press, 1988.

Douglas R. MacAyeal, Department of the Geophysical Sciences, The University of Chicago, 5734 South Ellis Avenue, Chicago, IL 60637.

(Received July 3, 1988;
revised September 20, 1988;
Accepted October 10, 1988.)